Bull. Mater. Sci., Vol. 28, No. 5, August 2005, pp. 395–399. © Indian Academy of Sciences.

Structure and coercivity of nanocrystalline Fe–Si–B–Nb–Cu alloys

B MAJUMDAR* and D AKHTAR

Defence Metallurgical Research Laboratory, P.O. Kanchanbagh, Hyderabad 500 058, India

MS received 5 February 2005; revised 24 February 2005

Abstract. Crystallization behaviour and magnetic properties of melt-spun Fe–Si–B–Nb–Cu alloys have been investigated. It is found that the primary phase changes from *a*-Fe(Si) to Fe_3Si (DO_3) on increasing the Si content. The coercivity of the alloys containing the Fe_3Si phase is significantly lower as compared to the alloy containing *a*-Fe(Si) phase. A heat treatment temperature–time–coercivity map has been obtained for optimization of the coercivity.

Keywords. Fe–Si–B–Nb–Cu alloy; melt-spinning; crystallization; nanocrystalline materials; coercivity.

1. Introduction

Nanocrystalline Fe–Si–B–Nb–Cu alloys have been found to possess a unique combination of soft magnetic properties including high saturation, very low coercivity, high permeability and high electrical resistivity (Yoshizawa *et al* 1988). These alloys are prepared by primary crystallization of amorphous precursors through an optimum annealing treatment. The obtained magnetic properties depend strongly on the microstructure and the phase composition of the primary nanocrystalline phase (He *et al* 1994; Tomic and Davidovic 1996). However, the microstructural evolution during heat treatment is not clearly understood.

Several different crystalline structures have been reported depending on the heat treatment conditions (Noh *et al* 1991; Lopez-Quintela *et al* 1992; Muller *et al* 1992; Rixecker *et al* 1992; Kim *et al* 1994). Noh *et al* (1991) studied the effect of Nb, Cu and combined addition of Cu and Nb on the crystallization behaviour and microstructural changes in Fe–Si–B melt spun alloys. Koster and Meinhardt (1994) studied primary crystallization of Fe–Si–B–Nb–Cu alloys and found that the growth of nanocrystals can be controlled by selecting proper composition. We have investigated the effect of Si content and melt spinning ambient on the evolution of nanocrystalline phases and the resultant magnetic properties in Fe–Si–B–Nb–Cu alloys. Results of these investigations are presented in this paper.

2. Experimental

Alloys of compositions, $Fe_{77.5}Si_{11.2}B_{7.2}Nb_{3.3}Cu_{0.8}$, $Fe_{73.2}Si_{13.7}B_{9.5}Nb_{2.7}Cu_{0.9}$ and $Fe_{68.8}Si_{18.6}B_{9.5}Nb_{2.6}Cu_{0.5}$, were prepared by melting the pure elements in a vacuum induction melting furnace. The alloys were designated as FIN-1, FIN-2 and FIN-3, respectively. Around 30–40 μm thick and 3–10 mm wide amorphous ribbons were obtained by melt spinning in argon/air using a vacuum melt spinning unit. Annealing treatment on ribbon samples was carried out in vacuum sealed quartz ampoules (2×10^{-4} mbar) at different temperatures ranging from 783–873 K. The annealing time was varied from 15–120 min at an interval of 15 min.

X-ray diffractometry (XRD) and differential scanning calorimetry (DSC) were employed to evaluate the structure and thermal stability of the alloy ribbons. Transmission electron microscopy (TEM) of the melt spun and heat treated samples was carried out using PHILIPS 430T transmission electron microscope. Samples for TEM investigations were prepared using PIPS–GATAN 691 precision ion polishing system. Coercivity of the as spun and heat treated samples was measured using FÖRSTER–KOERZIMAT 1·095 coercimeter.

3. Results

XRD spectra of the as spun ribbons of FIN-1, FIN-2 and FIN-3 alloys revealed a diffused intensity pattern, characteristic of amorphous phase. DSC thermograms of the melt spun alloys at a heating rate of 20 K/min are shown in figure 1. From the plots it is clear that the temperature of onset of crystallization (T_x) for FIN-1 alloy is around 788 K whereas FIN-2 and FIN-3 crystallize at a higher temperature of around 817 K.

XRD patterns of FIN-1 and FIN-2 ribbons heat treated at different temperatures viz. 783, 813, 843 and 873 K, for a period of 60 min revealed that partial crystallization of amorphous phase occurs on heating at lower temperature. Sharp reflections corresponding to crystalline phase start appearing and the diffused intensities, correspond-

*Author for correspondence (bhaskar@dmrl.ernet.in)

ing to the existence of amorphous phase are reduced with the increase in heat treatment temperature and finally vanish in the samples heat treated at 873 K. Figure 2 shows XRD patterns of FIN-1 and FIN-2 samples heat treated at 843 K for 60 min. It is interesting to note that heat treated samples of FIN-1 (figure 2a) show the evolution of *a*-Fe(Si) phase (*bcc*) whereas the primary phase for FIN-2 (figure 2b) samples is indexed to ordered Fe_3Si phase (DO_3).

Figure 3 shows TEM micrographs (bright field) and corresponding selected area diffraction (SAD) patterns of FIN-2 sample before and after heat treatment. The featureless contrast in microstructure and diffused rings in SAD pattern (figure 3a) confirms the presence of amorphous phase in the as quenched samples. One observes very fine clusters of size less than 3 nm; these can be frozen in nuclei during rapid solidification as suggested by Hono *et al* (1999).

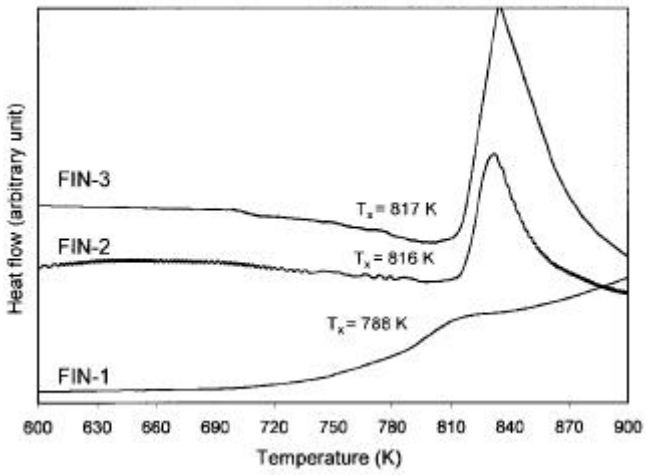

Figure 1. DSC plots for as spun ribbons of FIN-1, FIN-2 and FIN-3 alloys at a heating rate of 20 K/min.

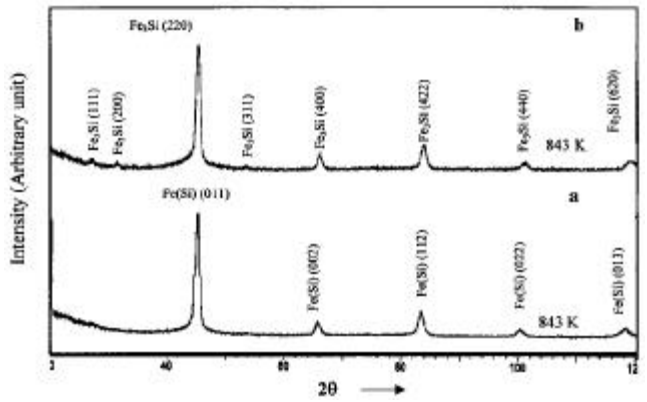

Figure 2. XRD patterns (CuK_a) of a. FIN-1 and b. FIN-2 ribbons heat treated for 60 min.

Figure 3b shows a typical TEM micrograph (bright field) of the sample heat treated at 798 K. The ring pattern in SAD (inset) corresponds to Fe_3Si phase. By increasing the heat treatment temperature the fraction of nanocrystalline grains increases at the expense of amorphous phase. No amorphous phase is left in the sample heat treated at 873 K (figure 3c). This can be visualized by comparing the SAD patterns of figures 3b and c; the diffuse ring corresponding to the presence of amorphous phase is visible in figure 3b along with the sharp rings whereas it is completely absent in figure 3c.

Figure 4 shows the average grain size measured from TEM micrographs and also calculated from the broadening of XRD peaks using Scherrer formula for different heat treatment temperatures. A straight line is fitted through regression analysis for both the cases. A shift of the curve to the higher values is observed for grain size obtained from TEM micrographs. This difference may be due to the incorporation of instrumental broadening in XRD patterns and/or overlapping of the nanocrystalline grains in TEM micrographs. Nevertheless, in both the cases, only a marginal increase in grain size is observed with increase in heat treatment temperature. The slopes of the fitted straight lines are found to be 0·02 and 0·016, respectively which indicates that grain size is almost stable within the range of heat treatment temperatures.

Figure 5 shows the variation of coercivity with heat treatment temperature for all the alloys. The coercivity of as melt spun alloys is also included in the figure. It is noteworthy that the coercivity of FIN-1 is almost an order of magnitude higher as compared to the other two alloys. The coercivity decreases from FIN-1 to FIN-3 which suggests that higher Si content leads to lower coercivity. For all the alloys, the coercivity initially decreases with heat treatment temperature up to 783 K, remains constant up to 843 K and then increases abruptly at higher temperature.

Figure 6 shows a heat treatment temperature–time–coercivity map for the FIN-2 alloy. It can be observed that there exists a basin where coercivity shows minimum value in heat treatment temperature–time axes. For low temperature (783 K) annealing, the time required to achieve low coercivity is higher and has a broad range (up to 120 min). On the other hand if the annealing temperature is high (873 K), the low coercivity can be achieved within 30 min beyond which the coercivity increases rapidly with the annealing time.

The investigations reported above were carried out on the ribbons prepared in an inert argon atmosphere after proper evacuation. To study the effect of melt spinning ambient, ribbons of FIN-2 alloy were also prepared in air. Structure, thermal stability and magnetic properties of these samples were found to be similar as for the samples prepared in inert atmosphere. It shows that the melt spinning ambient has no significant effect on the structure and magnetic properties of these alloys.

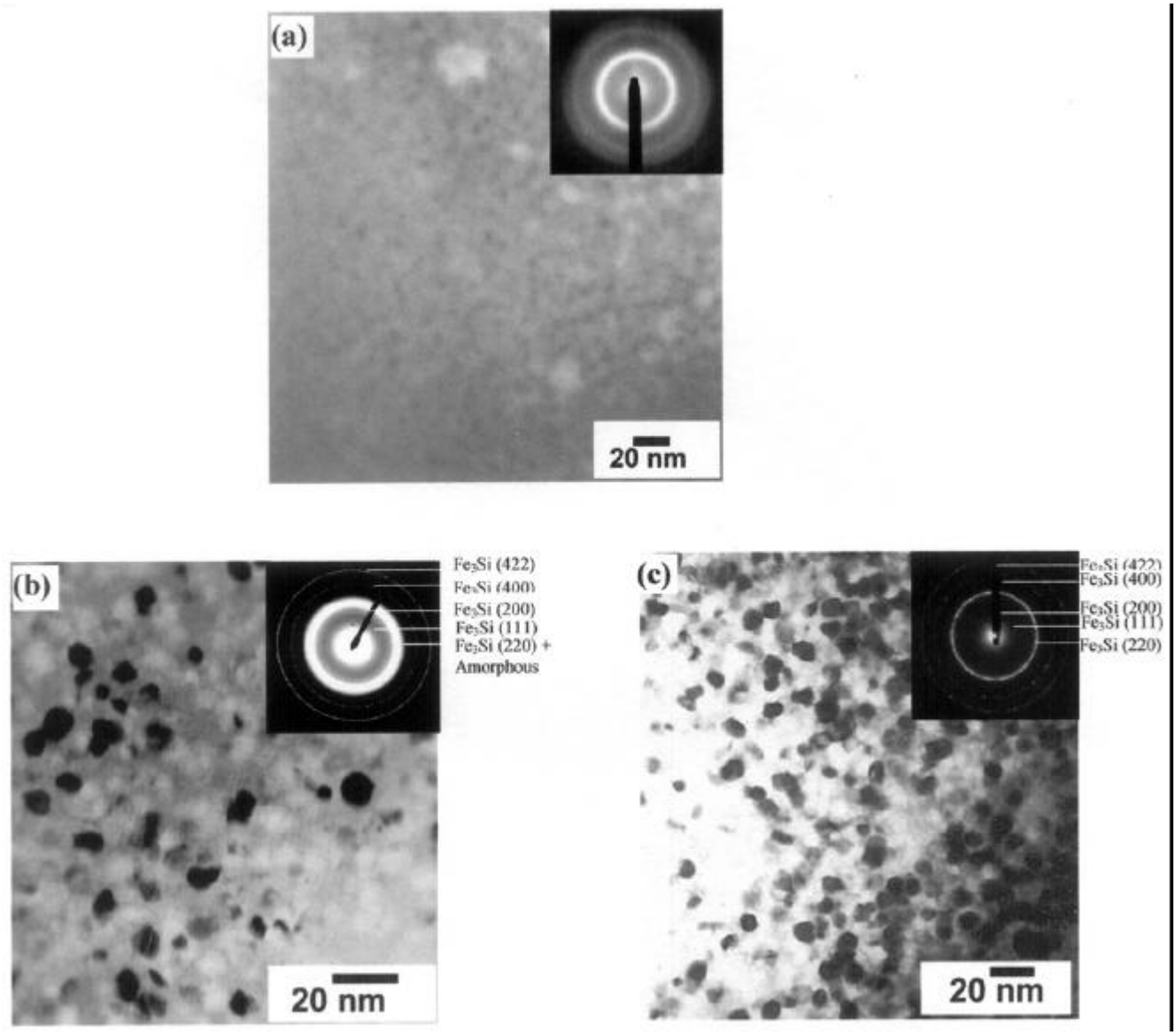

Figure 3. Bright field micrographs and corresponding SAD patterns (inset) of FIN-2 ribbons: (**a**) as melt spun, (**b**) heat treated at 798 K and (**c**) heat treated at 873 K.

4. Discussion

Our results indicate that on annealing, *a*-Fe(Si) nanocrystalline phase is formed in FIN-1 alloy (11·2 at% Si) whereas ordered DO_3–Fe_3Si phase is observed in the other alloys. Formation of primary phase in Fe–Si–B–Nb–Cu alloys is, therefore, dependent on Si content; beyond 11·2 at% Si, Fe_3Si phase stabilizes. It is interesting to note that the coercivity of the samples containing Fe_3Si phase is lower by an order of magnitude as compared to the FIN-1 alloy. The presence of nanocrystalline grains in amorphous matrix is observed in the samples heat treated even below the crystallization temperature. This implies heterogeneous nucleation occurring below T_x, in agreement with the observation of Hono *et al* (1999).

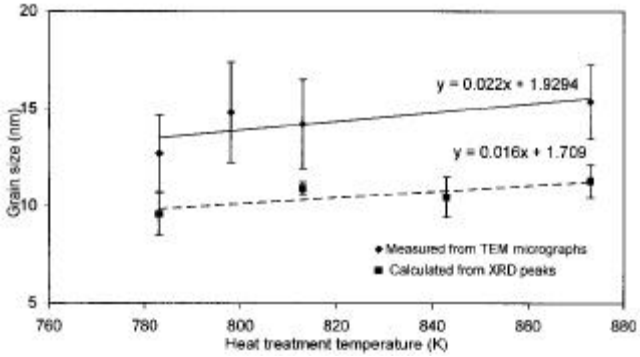

Figure 4. Grain size of primary phase as a function of heat treatment temperature (60 min).

Formation of nanocrystalline grains in the amorphous matrix after heat treating the samples leads to reduction of coercivity. Following Alben and Becker (1978) theory on random anisotropy model for amorphous phases, the effect of magnetocrystalline anisotropy will be averaged out and exchange interaction will dominate when the size of the crystallites is less than the exchange length which is limited to 35 nm in case of Fe–Si phase (Herzer and Hilzinger 1986). Moreover, positive contribution of amorphous phase and negative contribution of crystalline phase in magnetostriction lead to almost zero magnetostriction in the nanocomposite (Herzer 1991).

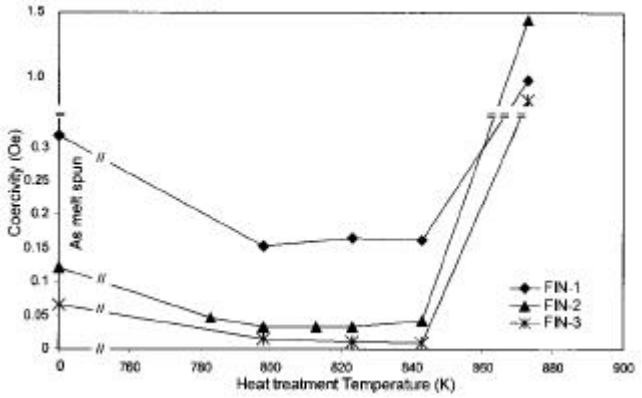

Figure 5. Coercivity as a function of heat treatment temperature (60 min).

Under the application of magnetic field, the exchange coupling between nanocrystals and amorphous phase takes place causing a large Barkhousen jump along the domain boundary. Coercivity does not vary as long as the coupling between grains and amorphous phase exists and grain size is uniform below the exchange length. This occurs between 798 and 843 K heat treated samples where the grain size has not altered significantly as well as the amorphous phase still exists within the intergranular region. Even though there is very little change in the size of nanocrystals at 873 K, abrupt increase of coercivity is due to the disappearance of amorphous phase in the intergranular region. Indeed, it has been found (Raja *et al* 2000) that mechanically alloyed Fe–Si–B–Nb–Cu alloys containing nanocrystalline Fe–Si phase possess higher coercivity as compared to the melt spun alloys because of the absence of intergranular amorphous phase.

Our results show that the coercivity decreases with increasing Si content in amorphous, partially crystallized as well as fully crystallized samples. Since magnetostriction plays a dominant role by contributing to the strain field under magnetization, the change in coercivity is attributed to the variation of magnetostriction with Si content. The results could be explained in terms of diminishing value of magnetostriction with Si as has been pointed out by Herzer (1997).

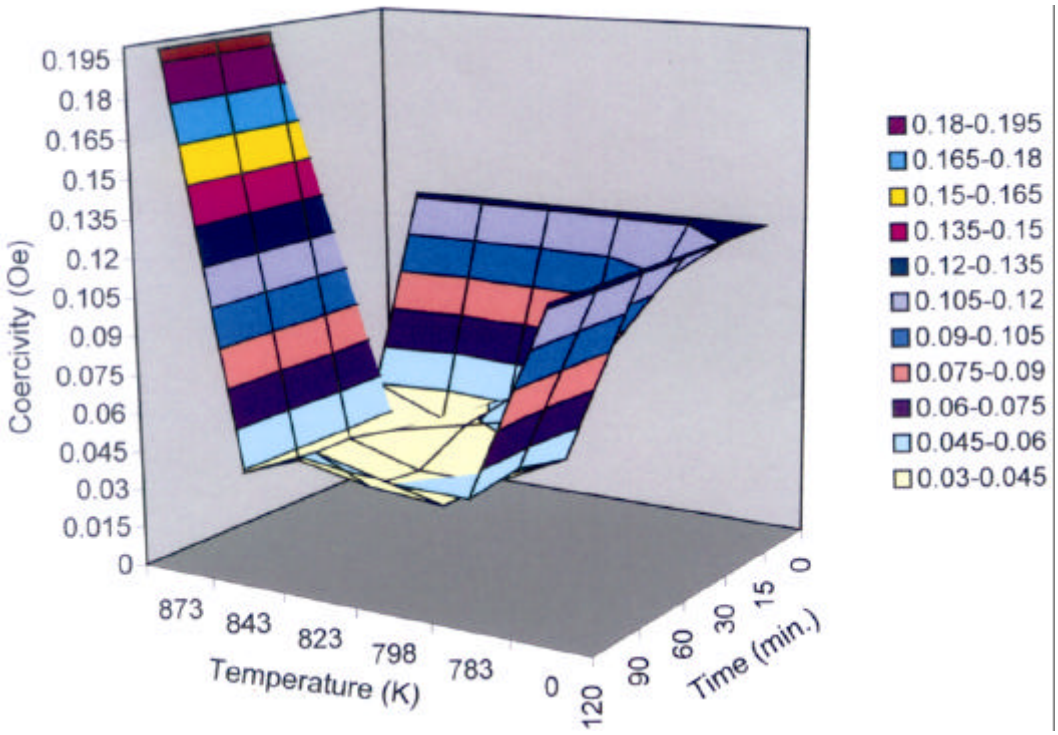

Figure 6. Heat treatment temperature–time–coercivity map for FIN-2 alloy.

5. Conclusions

Primary crystallization of amorphous Fe–Si–B–Nb–Cu alloy yields *a*-Fe(Si) phase at a Si content of 11·2 at% and Fe_3Si phase at higher Si contents. The coercivity of the alloys containing the Fe_3Si phase is an order of magnitude lower than that of the former. Melt spinning ambient has no significant effect on the structure and coercivity of the alloy. A heat treatment temperature–time–coercivity map has been established to obtain a basin of minimal coercivity.

Acknowledgements

Thanks are due to Prof. K Chattopadhyay, Dr V Chandrasekharan, Dr K Muraleedharan, Dr A K Singh and Dr H V Kiran, for their kind help and fruitful discussions. This work was supported by the Defence Research and Development Organization, Government of India. The authors are grateful to Dr A M Sriramamurthy, Director, DMRL and Dr D Banerjee, Chief Controller (R&D), for their continued support.

References

Alben R and Becker J J 1978 *J. Appl. Phys*. **49** 1653

He K Y, Sui M L, Liu Y and Zhao B F 1994 *J. Appl. Phys*. **75** 3684

Herzer G 1991 *Mater. Sci. Engg*. **A133** 1

Herzer G 1997 *Handbook of magnetic materials* (ed.) K H J Buschow (Amsterdam: Elsevier Science) Ch. 3, **Vol. 10** p. 415

Herzer G and Hilzinger H R 1986 *J. Magn. Magn. Mater*. **62** 143

Hono K, Ping D H, Ohnuma M and Onodera H 1999 *Acta Mater*. **47** 997

Kim W T, Jang P W, Yu S C and Chun B S 1994 *Mater. Sci. Engg*. **A179–180** 309

Koster U and Meinhardt J 1994 *Mater. Sci. Engg*. **A178** 271

Lopez-Quintela M A, Rivas J, Duro R J, Winter I and Bonome M G 1992 *J. Magn. Magn. Mater*. **112** 307

Muller M, Mattern N and Illgen L 1992 *J. Magn. Magn. Mater*. **112** 263

Noh T H, Lee M B, Kim H J and Kang I K 1991 *J. Appl. Phys*. **67** 5568

Raja M M, Chattopadhyay K, Majumdar B and Narayansamy A 2000 *J. Alloys Compounds* **297** 199

Rixecker G, Schaff P and Gonser U 1992 *J. Phys. Condens. Matter* **4** 10295

Tomic P and Davidovic M 1996 *J. Non-cryst. Solids* **204** 32

Yoshizawa Y, Oguma S and Yamauchi K 1988 *J. Appl. Phys.* **64** 6044